



Long Term Durability of Steel Reinforcements in Concrete Footpath Joints

Report Prepared By: Jay Sanjayan, PhD Professor of Concrete Structures Director of Centre for Sustainable Infrastructure Swinburne University of Technology Hawthorn, VIC 3122 Phone: 03 9214 8034 email: jsanjayan@swin.edu.au	Client: TripStop Pty Ltd PO Box 2438 Rowville VIC 3178 www.tripstop.net Phone: 1300 900 063
	 Date: 7 July 2014

Background

This report is written in response to a request by TripStop Pty Ltd to comment on the practice of using continuous steel reinforcement as dowels to prevent vertical movements along saw-cut joints.

Key Joints

Saw-cut joints in concrete footpaths are normally placed to accommodate shrinkage cracks and allow for horizontal movements of the concrete for thermal expansions and contractions. The vertical movements at these joints need to be prevented. Commonly used method of preventing the vertical movement is by a key joint. Typical detailing for this type of joints is shown in Figure 1 below:

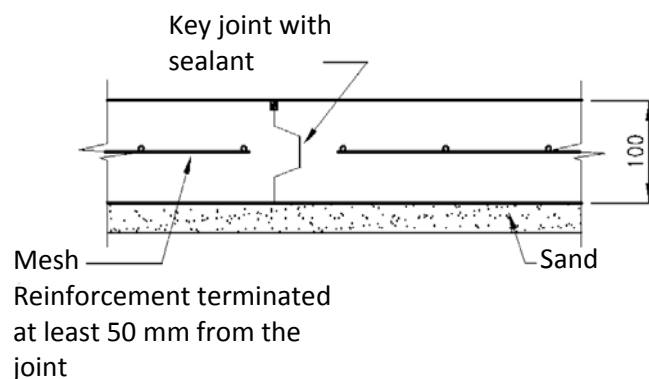


Figure 1: Key joints with Saw-cut

Hinge Joints (Tripstop)

The client of this report supplies a hinge joint, Tripstop. This joint works similar to a key-joint preventing vertical movements while avoiding continuous reinforcements through joint.

Steel Mesh Reinforcement as Dowels

The use of steel mesh reinforcement as dowels to control the vertical movements in saw-cut joint is shown in Figure 2. This practice is effective for foot paths that only require a short life, eg. less than 5 years. For foot paths that require longer life, eg. > 10 years, this method of placing mesh reinforcements all the way through the saw-cut joints is a bad practice since the steel reinforcement will corrode and there will be no effective vertical resistance to prevent the joint from sliding in vertical direction. This practice is effectively banned in the Australian Standard AS3727, where in Clause 8.3e it is clearly stated "Reinforcement should not be continuous through control joints".

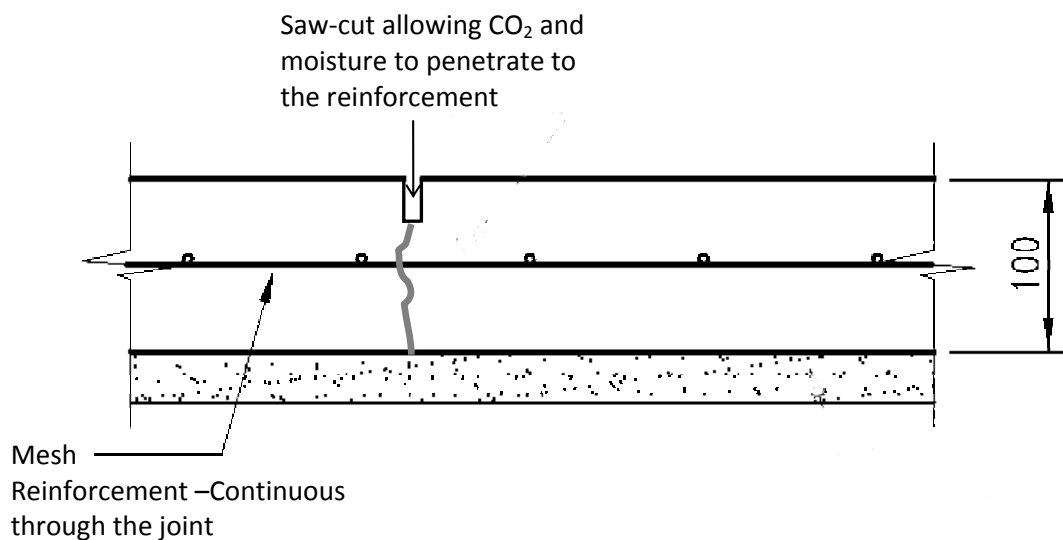


Figure 2: Steel Mesh Reinforcement as Dowel

Corrosion of steel reinforcements in concrete is normally protected by the alkaline environment provided by the surrounding concrete. Concrete normally provides a pH of greater than 13. This protection can be broken down by the infiltration of chlorides or carbon dioxide from the atmosphere. Carbon dioxide in the atmosphere will infiltrate through the saw-cut joint and through the induced crack resulting in neutralisation of the concrete in the vicinity. This process is termed as carbonation and is responsible for major maintenance costs in reinforced concrete infrastructure assets.

Chlorides are a major problem in coastal areas, but aerosols from the ocean have been found to be carried in the wind up to several kilometres inland. Carbonation or chloride penetrations into concrete typically take about 50 years to reach the steel reinforcement at which time the corrosion initiation will take place. Once the corrosion is initiated the steel will start corroding. The rate of corrosion depends on the oxygen and moisture availability in corroding areas.

The corrosion of reinforcements either due to carbonation or chloride ingress is a major infrastructure problem worldwide consuming large part of the maintenance budgets. This problem is colloquially known as concrete cancer.

Since the saw-cut joints trap moisture from the rain and allow oxygen through the saw-cut and induced crack, the rate of corrosion will be high. In these conditions, the loss of cross section of steel bars due to corrosion will be rapid, leading to loss of the steel bar's ability to transfer shear loads. The breakages of steel bars areas are likely to occur within a period of 5 to 10 years, depending on the environmental conditions.

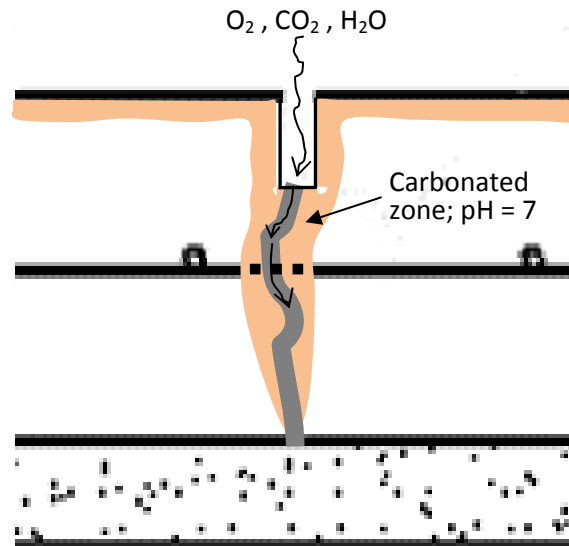


Figure 3 Carbonation of concrete and corrosion with the supply of Oxygen and Moisture

SL72 Steel Reinforcement Mesh

While SL72 mesh is sufficiently strong to reinforce the foot path concrete slab to give some robustness, it is far too small to provide the crack bridging if it is used for that purpose. The calculations below demonstrate the inadequacy of this reinforcement as it shows that the mesh SL72 would have yielded at the crack location within a short period of shrinkage (~50 days) and allow a crack opening in the range of 0.9 to 1.5 mm depending on the joint spacing.

The diameter of the SL72 mesh, $d_s = 6.75 \text{ mm}$

Area of steel bar = 35 mm^2

The spacing of the bars, $A_{st} = 200 \text{ mm}$

The depth of the slab, $d = 100 \text{ mm}$

The corresponding area of concrete for each bar, $A_c = 200 \times 100 = 20,000 \text{ mm}^2$

Steel ratio, $\rho = 35/20,000 = 0.175 \%$

Strength of concrete, $f'_c = 25 \text{ MPa}$

Elastic Modulus, $E_c = 26,700 \text{ MPa}$

Effective thickness of 100 mm deep slab, $t_h = 200 \text{ mm}$

Creep factor, $\phi_{cc} = 3.34$

Effective Elastic Modulus, $E_{eff} = E_c / (1 + \chi\phi_{cc}) = 26,700 / (1 + 0.8 \times 3.34) = 7,271 \text{ MPa}$

Tensile strength of concrete, $f_t = 0.4v f'_c = 2 \text{ MPa}$

Prior to cracking, tensile stress in the concrete, $\sigma_{cc} = \epsilon_{sh} \times E_{eff}$

At the time of cracking, $\sigma_{cc} = 2 \text{ MPa} = \epsilon_{sh} \times E_{eff} = \epsilon_{sh} \times 7,271$

Shrinkage at the time of first crack = $\epsilon_{sh} = 275 \mu\epsilon$

The long term shrinkage (including autogenous shrinkage) = $610 \mu\epsilon$

The first crack will occur around 50 days after the concrete placement.

The minimum steel reinforcement area required to bridge the crack (to take up the tensile stress carried by the concrete), $A_{st,min}$:

$$A_{st,min} \times f_{sy} = A_c \times f_t$$
$$A_{st,min} \times 500 = 20,000 \times 2$$
$$A_{st,min} = 80 \text{ mm}^2$$

To satisfy the minimum steel mesh requirement it would take 3 Nos of SL72 or other larger size mesh.

One SL72 will yield at the time of first cracking around 50 days after casting the concrete.

Once yielded, the steel reinforcement will keep yielding to accommodate for the long term shrinkage.

The long term shrinkage is around 610 $\mu\epsilon$.

For joints at a spacing of 1.5 m, the crack opening due to this shrinkage will be:
 $= 1500 \times 610 \times 10^{-6} = 0.9 \text{ mm}$

The joint spacings of 2 and 2.5 m are also commonly used. The following cracks widths are calculated for these joint spacings:

Joint Spacing	1.5 m	2.0 m	2.5 m
Estimated Crack Width	0.9 mm	1.2 mm	1.5 mm
Area loss due to corrosion	45%	60%	75%

Crack widths more than 0.1 mm is large enough to allow atmospheric carbon dioxide to cause carbonation of concrete in the vicinity of the steel mesh and initiate corrosion as soon as the crack opened. The availability of oxygen and moisture will cause rapid corrosion of steel mesh leading to failure which is estimated to be around 5 to 10 years. Estimated area loss of steel bars by a method proposed by Vidal et al (2004) is also presented in the table above.

Further, SL72 is a low ductility steel. It only has an elongation capacity of 1.5%. If the bond length is about $12d_s$ (a commonly assumed figure), the elongation requirement to accommodate 1.2 mm crack opening is $= 1.2 / (12 \times 6.75) = 1.5\%$. The elongation capacity of low ductile SL72 is on the borderline of being able to accommodate the elongation requirement demanded by the crack opening. Once the elongation capacity is exhausted, the steel will snap with further shrinkage or thermal contraction of the concrete.

MTS Test Report

The MTS report (MT-14/158) shows the test results of slabs, one with mesh reinforcement and the other with Tripstop joints. The results demonstrate that the Tripstop hinge-joint was able to accommodate larger displacement in cycle 1. With cycles 2 and 3, the displacements were comparable.

The mesh reinforcement was able to accommodate the differential displacement due to the significant aggregate interlock occurred in the test. This result is due to the particular test

arrangement which is not representative of the field conditions and cannot be relied upon for the field performance. The reasons for this are explained below:

(1) Degree of aggregate interlock is random; the crack is created by shrinkage not by uplift force

In the test, the concrete is cracked by the lifting force. In the field conditions, the concrete in saw-cut joints will first be cracked by shrinkage of slabs which is expected to happen about 2 months after the initial casting of the slab as demonstrated by the calculations above (50 days). The cracked shape created by shrinkage will not necessarily be as rugged as the crack forced upon by the lifting force simulated in the test. Further, the shape of the crack is random depending on the aggregates positioned in the saw-cut joints. Sometimes the crack formed during shrinkage phase can be straight offering no aggregate interlock whereas other times it may be rugged. This random nature of the shape of the crack should not be relied upon as this is not repeatable.

(2) Loss of aggregate interlock over time due to the widening of the saw-cut joints

The heave is expected to occur in the field conditions some years after the initial slab construction. By this time, the saw-cut joint would have widened significantly (in the range of 0.9 to 1.5 mm as the above calculations demonstrate). When the heave occurs after the crack has formed and widened, the aggregate interlock may not exist as found in the test. In the test, there is no time allowed for the shrinkage to occur and the crack to widen before the uplift force was applied.

(3) Thermal expansion/contraction and creep effects

The joints are supposed to take care of the thermal expansion and contraction of the concrete slab. Under these daily temperature cycles, the aggregate interlock will be loosened over time. Further, creep of concrete, which is a long term relaxation of concrete under stress, will allow the aggregate interlock to loosen over time. These phenomena are not included in the test. Therefore, the aggregate interlock effect found in the test is peculiar to the test condition and not representative of the field condition.

Conclusions

Use of steel mesh reinforcement to provide dowel action to stop vertical sliding in saw-cut joints is a bad practice which places large capital investments in footpath constructions into high risk of incurring large maintenance costs due to corrosion of reinforcements (colloquially known as concrete cancer).

Research carried out by leading engineers from the University of California, Berkeley (USA) is attached (Mancio et al 2008). This research shows that ordinary carbon steel will corrode in this type of scenario and is inadequate for this application. Other types of steels, such as stainless steel or epoxy coated steel reinforcement are recommended for this application. This research paper is published in the prestigious journal from the ASCE (American Society of Civil Engineers).

In the short-term test by MTS, the aggregate interlock appears to be effective. This is a random effect and should not be relied upon. Shrinkage of concrete overtime will widen the saw-cut joint and the aggregate interlock in the widened crack may not exist as seen in the test condition. Further, thermal expansion and contraction due to day and night temperature cycles will loosen any aggregate interlock that may be initially present. Creep of concrete which is a relaxation phenomenon also loosen the aggregate interlock overtime.

References

Mancio, M., Carlos, C., Zhang, J., Harvey, J.T., Monteiro, P.J.M. and Ali, A., "Evaluation of Corrosion Resistance of Steel Dowels Used for Concrete Pavements", *Journal of Materials in Civil Engineering*, ASCE, Vol. 20, No. 10, October 1, 2008, pp. 650 – 658.

AS3727, "Guide to residential pavements", Standards Australia, first published 1993.

Vidal, A., Castel, R., Francois, R., "Analysing crack width to predict corrosion in reinforced concrete", *Cement and Concrete Research*, Vol.34, No. 1, January 2004, pp. 165–174.

Evaluation of Corrosion Resistance of Steel Dowels Used for Concrete Pavements

Mauricio Mancio¹; Cruz Carlos Jr.²; Jieying Zhang³; John T. Harvey⁴; Paulo J. M. Monteiro⁵; and Abdikarim Ali⁶

Abstract: In concrete pavements, steel dowels are exposed to a particularly aggressive environment that leads to depassivation and greatly reduces the corrosion initiation stage. Aggressive agents such as chlorides and CO₂ have easy access to the dowels through pavement joints and, consequently, the corrosion performance of the system depends largely on the properties of the steel dowel being used. This study investigates the corrosion performance of several types of steel dowels embedded in concrete and subjected to accelerated corrosion by exposure to 3.5% NaCl solution for 18 months. Seven types of dowels were tested: bare carbon steel, stainless steel clad, grout-filled hollow stainless steel, microcomposite steel, carbon steel coated with bendable epoxy, and carbon steel coated with nonbendable epoxies. Half-cell potential, polarization resistance, visual inspections, and microscopic investigations by scanning electron microscopy were carried out to evaluate their corrosion performance. Results show that microcomposite steel dowels exhibit greater resistance to corrosion propagation than carbon steel dowels, but lesser than stainless clad and stainless hollow bars. In epoxy-coated bars, corrosion occurred at a few localized defective areas, generally at holidays and edges of bar ends. No significant difference was observed between nonbendable and bendable epoxy-coated dowels.

DOI: 10.1061/(ASCE)0899-1561(2008)20:10(650)

CE Database subject headings: Concrete pavements; Durability; Steel; Corrosion; Dowels.

Introduction

Steel dowels are used in jointed concrete pavements to provide load transfer across transverse joints. Their use reduces vertical deflections that cause faulting and stresses that cause corner and longitudinal cracking, by transferring part of the load to the unloaded slab. However, a number of problems can be created if there is corrosion of the dowels, and these problems can compromise the performance of the pavement and lead to pre-

mature failure (Harvey et al. 2003). These include the loss of dowel cross section, which reduces the capability of the dowel to transfer loads and restrain vertical movement, and the accumulation of corrosion products, which can induce tensile stresses in the concrete and also restrict the free expansion and contraction of the slabs, causing joint lockup and inducing cracks in the pavement.

It is well known that steel reinforcement in concrete is protected from corrosion by a passive film formed due to the high pH of concrete pore solutions, which slows the corrosion reaction rate to negligible levels, e.g., 0.1 $\mu\text{A}/\text{cm}^2$. The disruption of this passive layer—which typically happens as a result of the penetration of aggressive agents such as chloride ions (Cl⁻) and carbon dioxide (CO₂)—marks the end of the corrosion initiation stage and the onset of the propagation phase, as defined by Tuutti (1982). In concrete pavements the steel dowels are exposed to a particularly aggressive environment that leads to depassivation and greatly reduces the corrosion initiation stage. Aggressive agents such as chlorides and CO₂ have easy access to the dowels through the pavement joints, and may also access the full length of the bars because the bond between the dowels and concrete is designed to be tight, but to have low friction, which permits easier transport of the aggressive agents along the dowel than along a rebar. Chlorides are routinely used for ice control on highways in mountainous regions. Thus, the corrosion performance of the system depends largely on the properties of the steel dowel being used.

The main objective of this study is to investigate the corrosion performance of several types of steel dowels embedded in concrete that are subjected to environmental conditions intended to accelerate corrosion by exposure to concentrated chloride solutions.

¹Ph.D. Candidate, Dept. of Civil and Environmental Engineering, Univ. of California, Berkeley, 115 Davis Hall, Berkeley, CA 94720 (corresponding author). E-mail: mancio@berkeley.edu

²Ph.D. Candidate, Dept. of Civil and Environmental Engineering, Univ. of California, Berkeley, Berkeley, CA 94720. E-mail: ccj@berkeley.edu

³Ph.D. Research Associate, Institute for Research in Construction, National Research Council of Canada, Ottawa, ON Canada. E-mail: jieying.zhang@nrc-cnrc.gc.ca

⁴Associate Professor, Dept. of Civil and Environmental Engineering, Univ. of California, Davis, CA. E-mail: jtharvey@ucdavis.edu

⁵Professor, Dept. of Civil and Environmental Engineering, Univ. of California, Berkeley, CA 94720. E-mail: monteiro@ce.berkeley.edu

⁶Development Engineer, Pavement Research Center, Dept. of Civil and Environmental Engineering, Univ. of California, Davis, CA. E-mail: atali@ucdavis.edu

Note. Associate Editor: Byung Hwan Oh. Discussion open until March 1, 2009. Separate discussions must be submitted for individual papers. The manuscript for this paper was submitted for review and possible publication on June 21, 2006; approved on May 21, 2007. This paper is part of the *Journal of Materials in Civil Engineering*, Vol. 20, No. 10, October 1, 2008. ©ASCE, ISSN 0899-1561/2008/10-650-658/\$25.00.

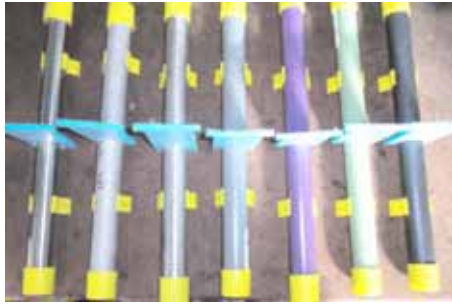


Fig. 1. Different types of steel dowels investigated. From left to right: microcomposite steel, stainless steel hollow, stainless steel clad, nonbendable epoxy-coated dowel (gray coating), nonbendable epoxy-coated dowel (purple coating), bendable epoxy-coated dowel (green coating), and bare carbon steel.

Materials and Methods

Seven types of steel dowels were evaluated for their corrosion performance: bare carbon steel, stainless steel clad, grout-filled hollow stainless steel, microcomposite steel, carbon steel coated with bendable epoxy [green color code (ASTM 2007a)], and carbon steel coated with nonbendable epoxies [purple and gray color codes (ASTM 2004)].

The stainless steel hollow dowels consist of a hollow type 316 stainless steel cylinder with approximately 5-mm-thick walls, filled with a cementitious grout. The stainless clad bars have a core of carbon steel covered by an outer layer (about 5-mm thick) of Type 316 stainless steel. The ends of the dowels do not have stainless steel cladding, but do have a protective paint coat. Microcomposite steel refers to microstructurally designed chromium-containing steels with an austenite-martensite structure that is virtually carbide free. Conventional carbon steels have mostly ferrite-carbide microstructures. In corrosive environments, these carbides become cathodic to ferrite and can develop microgalvanic corrosion cells, which can lead to accelerated corrosion. Due to the elimination of such microgalvanic cells, microcomposite steels are expected to be more resistant to corrosion (Trejo 1997; Trejo et al. 2000). In this study, the microcomposite steel specimens presented about 9% chromium, according to information provided by the manufacturer.

In order to facilitate the identification of corroded areas in the epoxy-coated dowels and evaluation of the role of defects on the development of localized corrosion, the epoxy coated dowels were checked for holidays (pinholes, voids, defects, etc.) before casting in the concrete beams. A low voltage holiday detector tester was used in accordance with ASTM G62 (ASTM 2007b). This mapping of original coating defects was used to check against possible locations of corrosion to be identified during the visual inspections of dowels after conditioning.

All dowels measured 38.1 mm (1.5 in.) in diameter and 460 mm (18 in.) in length, except for the microcomposite steel dowels, which had a diameter of 31.75 mm (1 1/4 in.). Before casting, electrical connections were made to one end of the steel bars and insulated with an epoxy mix, plastic expansion end caps were placed on both ends of the bars, and the dowels were mounted on plastic chairs (Fig. 1). In the middle of the concrete beam, a Styrofoam spacer was used to simulate a joint, and removed after the concrete had hardened. The steel dowels were cast in concrete beams measuring 150 × 150 × 560 mm

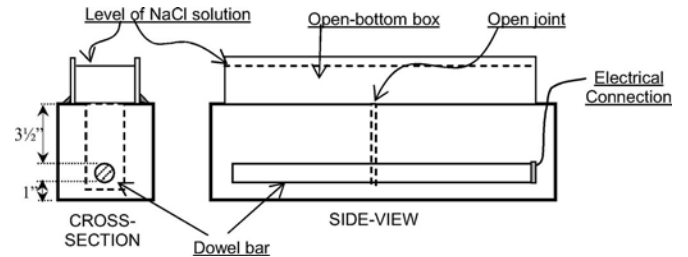


Fig. 2. Experiment setup to accelerate corrosion using chloride ponding

(6 × 6 × 22 in.). A relatively permeable concrete mix was used with a water-to-cement ratio of 0.65 and mix proportions 1:3.0:3.25 (cement: sand: gravel). Type I/II cement was used, and the maximum aggregate size was 12.8 mm (0.5 in.). The specimens were demolded 24 hours after casting and cured at 23 °C and 100% relative humidity (RH) for 28 days. Fig. 2 shows a schematic representation of the concrete specimens. Corrosion was accelerated by exposing the samples to weekly wet and dry cycles of a 3.5% NaCl solution at room temperature for a period of 18 months.

Half-cell potential tests, linear polarization resistance (LPR) curves, visual inspections, and microscopic investigations by scanning electron microscopy (SEM) were carried out to evaluate the corrosion performance of the dowels. Four replicates of each type of steel dowel were tested in this study.

Detection Techniques

Several electrochemical methods have been used to evaluate corrosion activity of steel reinforcement. The half-cell potential and the linear polarization resistance methods are among the most commonly used and accepted test methods for in situ measurements. These tests are easy to perform in the field and commercial instruments are readily available. Among the many methods that have been investigated for measuring the in situ corrosion rate of steel embedded in concrete, the linear polarization resistance appears to be gaining the most acceptance (Carino 1999). The half-cell potential method is indicative of the probability of corrosion activity of the reinforcing steel located beneath the half cell, and is described by ASTM C 876 (ASTM 1999). The setup basically consists of an external copper/copper sulfate (Cu/CuSO₄) electrode (half cell), connecting wires and a high impedance voltmeter (impedance > 10 MΩ). A high impedance voltmeter is necessary so that there is very little current through the circuit. The half-cell potential measurement has been widely used in the field due to its simplicity and general agreement among researchers that this technique effectively indicates the existence of active corrosion along the steel reinforcement in concrete. Table 1

Table 1. Relationship between Half-Cell Potential and Corrosion of Steel Embedded in Concrete (Adapted from ASTM C876)

Half-cell potential (mV) ^a	Corrosion interpretation
> -200	Low probability (10%) of corrosion
-200 to -350	Corrosion activity uncertain
< -350	High probability (90%) of corrosion

^aMeasurements made with a Cu/CuSO₄ electrode.

Table 2. Relationship between Corrosion Current Density and Corrosion Rate

Corrosion current density, i_{corr} ($\mu\text{A}/\text{cm}^2$)	Corrosion rate
<0.1	Negligible
0.1–0.5	Low
0.5–1.0	Moderate
>1.0	High

illustrates the relationship between measured potential and the likelihood of corrosion activity. The half-cell potential method, however, does not give any indication of the rate of corrosion on the steel.

The LPR technique is a well-established method for determining the rate of corrosion. The technique basically involves measuring the change in the potential of the electrolytic cell when an external current is applied to the cell, or vice versa. For a small perturbation about the open-circuit potential, there is a linear relationship between the change in applied current per unit area of electrode (Δi) and the change in the measured potential (ΔE). The ratio $\Delta E/\Delta i$ is called the *polarization resistance* (R_p). The corrosion rate, expressed as the corrosion current density (i), is inversely related to the polarization resistance, as indicated by the Stern–Geary relationship $i=B/R_p$, where B is a constant (ASTM 2003). Some guidelines have been developed to establish a relationship between corrosion current density and corrosion rate, as shown in Table 2 (Broomfield 1997).

A major concern with this method is the uncertainty about the area of the steel bar that is affected by the current from the counterelectrode (CE). Usually, it is assumed that the current flows in straight lines perpendicular to the bar and the counterelectrode, and the affected bar area is understood to be the bar circumference multiplied by the length of the bar below the counterelectrode, which in fact is not usually the case. However, in

the laboratory experiments performed in this study this concern is not justified, since virtually all the current will flow through the NaCl solution present in the open joint, which represents a very low-resistivity path as compared to concrete. As previously stated, the salt solution was removed from the concrete surface in order to perform the electrical measurements, but the joint remained filled with solution to provide this low-resistivity path for current flow. Note that the CE was placed just above the fabricated joint. Thus, it has been assumed that the area polarized corresponds to that part of the dowel exposed to the NaCl solution inside the fabricated joint. In this study, the linear polarization experiments were performed using a Princeton Applied Research model 263 potentiostat-galvanostat.

In addition to electrochemical measurements, visual inspections were conducted and a microstructural investigation was performed on the corroded dowels using SEM. The microstructural investigation was performed with a Digital Leo 430 scanning electron microscope using secondary electrons. The SEM imaging consists of bombarding the sample with an electron beam with sufficient energy to excite and eject secondary electrons, which are detected and recorded using a charge-coupled device (CCD) camera. In this study, samples of each corroded dowel type were collected during the visual inspection and then analyzed by SEM, with preference given to the inspection of the corroded areas in each sample.

Experimental Results and Discussion

Fig. 3 presents the linear polarization resistance plots for the carbon steel, microcomposite, hollow stainless steel, and stainless steel clad bars, respectively. The plots present the average results of four replicates normalized with respect to the half-cell value, in order to facilitate plotting and comparison among the different

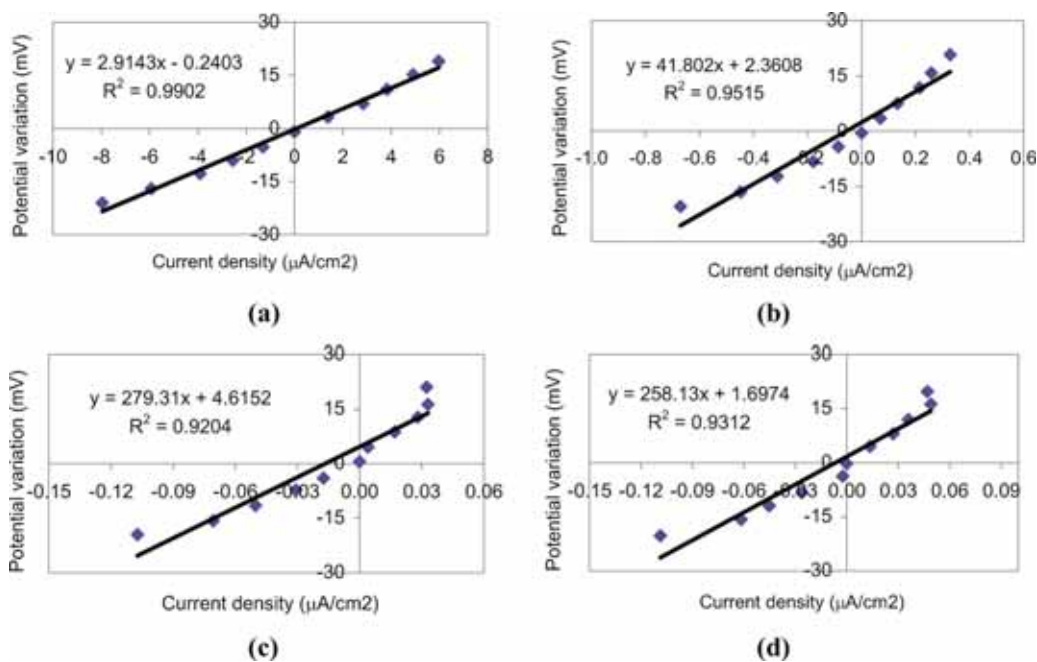


Fig. 3. Linear polarization results for: (a) carbon steel dowels; (b) microcomposite steel dowels; (c) stainless steel clad dowels; and (d) stainless steel hollow dowels

Table 3. Summary Results of Half-Cell Potential and LPR Tests

Specimen number		Half cell (mV)	R_p ($\Omega \text{ cm}^2$)	i_{corr} ($\mu\text{A}/\text{cm}^2$)
Carbon steel	1	-602	1,544.3	16.84
	2	-640	6,066.5	4.29
	3	-694	2,568.2	10.12
	4	-629	5,410.8	4.81
	Avg.	-641.3	3,897.5	9.01
	Std. dev.	38.6	2,183.2	5.84
Microcomp. steel	1	-567	23,495	1.11
	2	-571	23,146	1.12
	3	-292	367,410	0.07
	4	-278	124,620	0.21
	Avg.	-427.0	134,667.8	0.63
	Std. dev.	164.1	162,343.7	0.57
Stainless clad	1	-286	311,560	0.08
	2	-179	249,520	0.10
	3	-216	361,130	0.07
	4	-345	216,530	0.12
	Avg.	-256.5	284,685.0	0.09
	Std. dev.	73.8	64,414.8	0.02
Stainless hollow	1	-210	229,850	0.11
	2	-569	192,840	0.13
	3	-193	481,700	0.05
	4	-320	233,050	0.11
	Avg.	-323.0	284,360.0	0.10
	Std. dev.	173.4	132,819.5	0.03
Purple epoxy coating (nonbendable)	1	-476	—	—
	2	-582	—	—
	3	-464	—	—
	4	-811	—	—
	Avg.	-583.3	—	—
	Std. dev.	160.8	—	—
Gray epoxy coating (nonbendable)	1	-630	—	—
	2	-405	—	—
	3	-648	—	—
	4	-597	—	—
	Avg.	-570.0	—	—
	Std. dev.	112.0	—	—
Green epoxy coating (bendable)	1	-420	—	—
	2	-760	—	—
	3	-558	—	—
	4	-643	—	—
	Avg.	-595.3	—	—
	Std. dev.	143.2	—	—

specimens of a given sample. Individual half-cell potentials for each specimen are presented in Table 3. Current density (in $\mu\text{A}/\text{cm}^2$) and potential (in mV) are given as variations from the values obtained at equilibrium (i.e., at half-cell potential). The slope of the curves ($\Delta E/\Delta i$) provides the value of the polarization resistance, R_p . Notice that the greater the slope, the more difficult the charge transfer across the metal/electrolyte interface—therefore the corrosion current density is lower and, consequently, the corrosion reaction rate is slower.

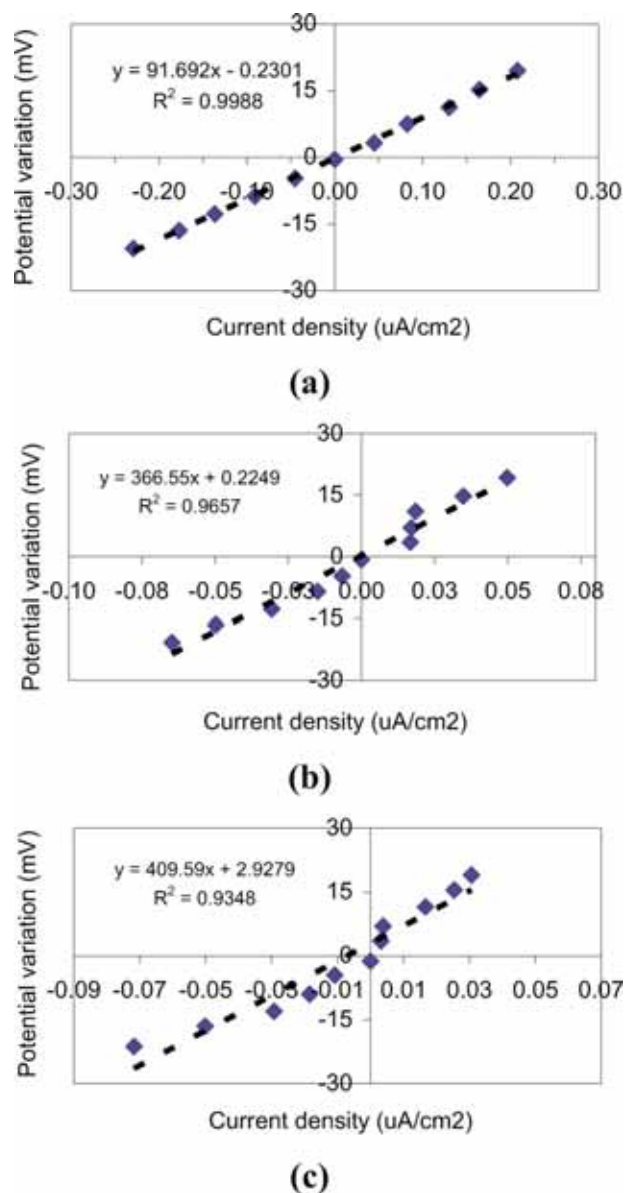


Fig. 4. Linear polarization results for: (a) nonflexible epoxy-coated dowels (purple colored); (b) nonflexible epoxy-coated dowels (gray colored); and (c) flexible epoxy coated dowels (green colored)

It can be seen that for the same variation in potential, carbon steel bars exhibit a much larger variation in the corrosion current density compared to the other materials. Therefore, the carbon steel samples will exhibit a smaller slope, smaller polarization resistance, and larger corrosion rate, followed by micro-composite steel, stainless steel clad, and stainless steel hollow, respectively.

Fig. 4 presents linear polarization resistance plots for the epoxy coated bars: nonflexible (purple and gray) and flexible (green) epoxy coatings. Note that the results obtained for the epoxy-coated bars are *not* to be interpreted quantitatively. The fact that electrical contact can be made between the reference electrode (copper/copper sulfate) and the working electrode (steel dowel), and that a half-cell potential can be measured for epoxy-coated bars, does indicate however the presence of defects in the coating. In coated specimens, corrosion is not uniform; instead, it is concentrated at localized defective areas (such

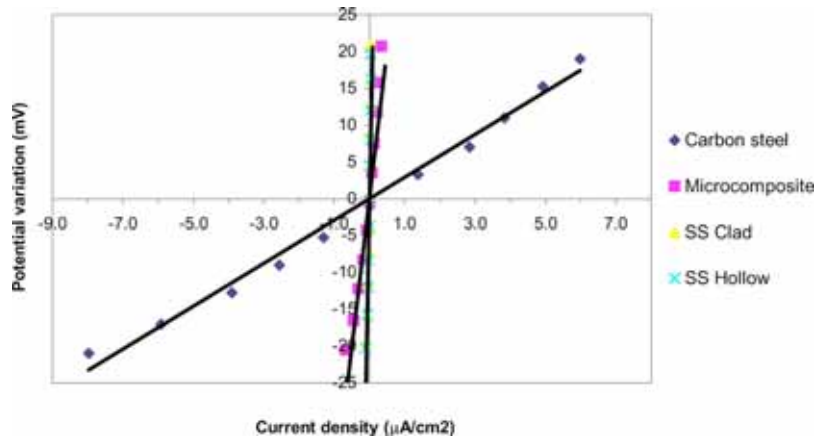


Fig. 5. Summary plot showing variation of potential and current density about half-cell potential, for different dowels

as pinholes, voids, etc.). Given that epoxy is an electrical insulator, polarization only occurs at these defective areas, which cannot be accounted for in the calculation of the polarization resistance term. As mentioned before, it has been assumed that the polarized area corresponds to the surface of the dowels exposed to the NaCl solution inside the fabricated joints. Note that if the polarized area is smaller than what is assumed, the actual corrosion current density (given in $\mu\text{A}/\text{cm}^2$) will be greater than what is calculated. As a result, the polarization results may indicate the presence of corrosion in the defective areas, but an evaluation of the extent of corrosion must rely on visual inspections

and microscopic investigations, which are presented in the next section.

Fig. 5 presents a comparison of the linear polarization results of various dowels. As mentioned above, the steeper the slope, the greater the corrosion resistance, R_p . It can be easily seen that the carbon steel specimens performed much poorer than the other dowels tested. On the other hand, the stainless steel hollow bars exhibited the best performance, followed by stainless steel clad and microcomposite steel dowels. Fig. 6 presents a comparative summary of polarization resistance and current density results, illustrating the average numerical values of R_p and i_{corr}

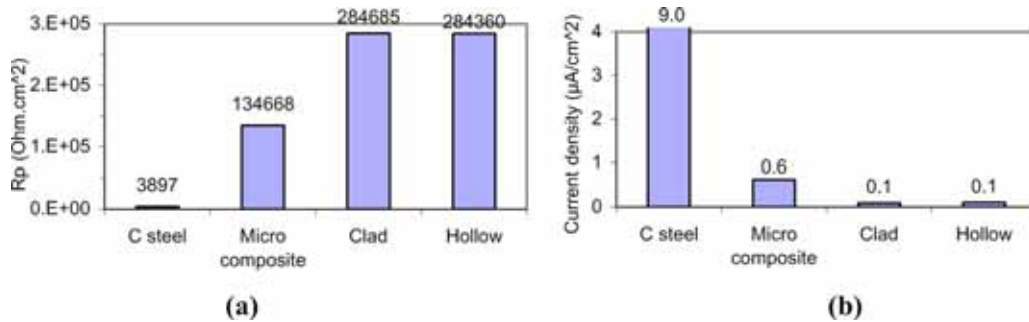


Fig. 6. Comparative column plots showing average results of polarization resistance (R_p) and corrosion current density (i_{corr}) for noncoated dowels

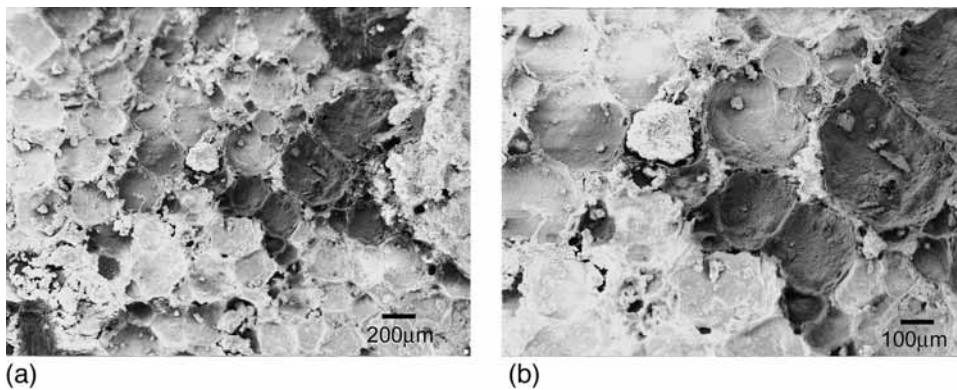


Fig. 7. Carbon steel samples: (a) heavy corrosion along dowel surface, magnification (Mag)=100×; (b) same region, Mag=200×

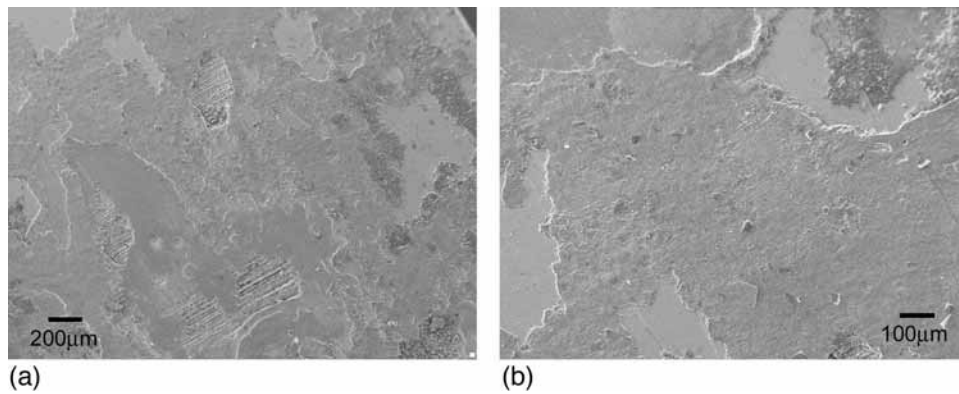


Fig. 8. Microcomposite steel samples: (a) aspect of corrosion along surface, Mag=100×; (b) same region, Mag=205×

obtained for the different samples. Table 3 summarizes the individual results obtained for each specimen including half-cell potential, polarization resistance (R_p), and corrosion current density (i_{corr}). Statistical analysis of the results was performed using the analysis of variance (ANOVA) model, and in all cases the type of steel dowel had a statistically significant effect on the parameters studied, i.e., half-cell potential, polarization resistance, and corrosion current density. Regarding the half-cell potential values, note that the stainless steel hollow and stainless steel clad specimens are, on average, located in the uncertain corrosion region, while all the other samples are in the active corrosion region (see Table 1). With respect to the corrosion current density, one can observe that the carbon steel dowels exhibited very rapid corrosion while microcomposite steel showed a moderate level of corrosion. Stainless steel clad and stainless steel hollow dowels proceeded at a low corrosion rate (refer to Table 2 for criteria used). The average values presented for the epoxy coated bars also indicate a low corrosion rate and, in fact, visual inspection revealed no major signs of corrosion for these dowels.

In addition, based on visual inspections, it was observed that the carbon steel samples were heavily corroded, the microcomposite steel dowels presented less corroded areas, and the stainless steel clad and stainless steel hollow dowels presented essentially no visible signs of corrosion. Defects were observed in the epoxy-coated bars and, as expected, the occurrence of localized corrosion in the defective regions was verified.

Microstructural Analysis of Corroded Areas

Figs. 7–13 present characteristic SEM images for each material investigated. In general, the severity of the corrosion observed by electron microscopy matches the results obtained by the electrical measurements and visual inspections. However, one should keep in mind that the microstructural investigation focused mostly on the corroded areas of each sample, and does not represent the general state of the dowel bars. The stainless steel clad dowels, for example, exhibited excellent performance on the corrosion rate measurements, and no corrosion was identified by visual inspection; however, relatively severe localized corrosion was observed at the uncoated but painted ends of the dowels, close to the interface with carbon steel.

A similar situation occurred with the analysis of epoxy-coated samples. It has been observed that the electrical measurements do not provide a reliable quantitative estimate of the corrosion state of epoxy-coated specimens, and in the visual inspection it was found that the bars were still in relatively good condition, especially as compared to carbon steel dowels. However, several defects on the epoxy coating have been observed, and their relation to the occurrence of localized corrosion has been explored. Unlike the microscopic analysis, half-cell and LPR measurements only provide general, averaged information about the corrosion state when uniform corrosion is assumed, and are not able to determine the corrosion pattern (uniform or localized). How these

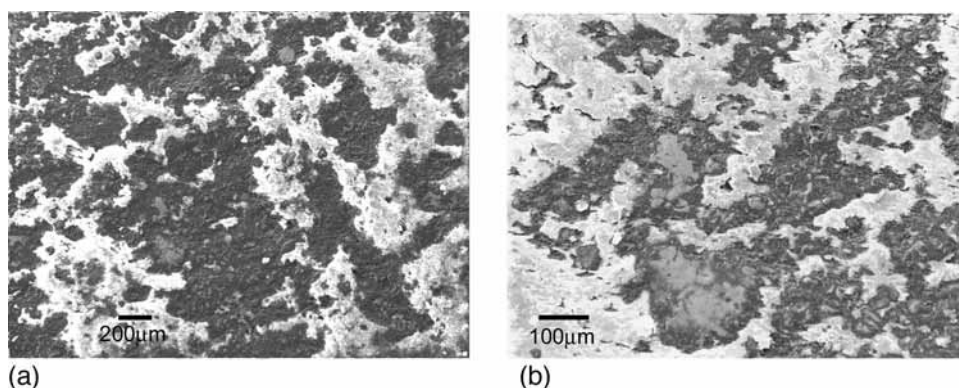
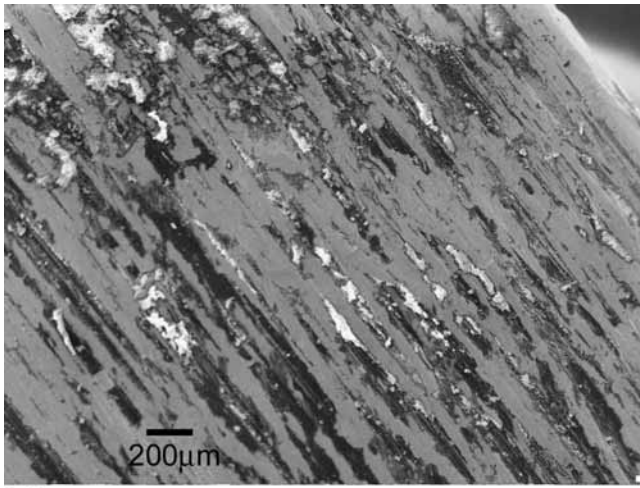
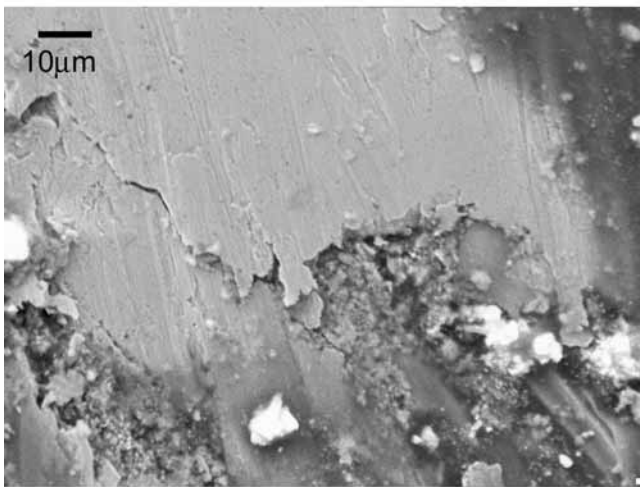


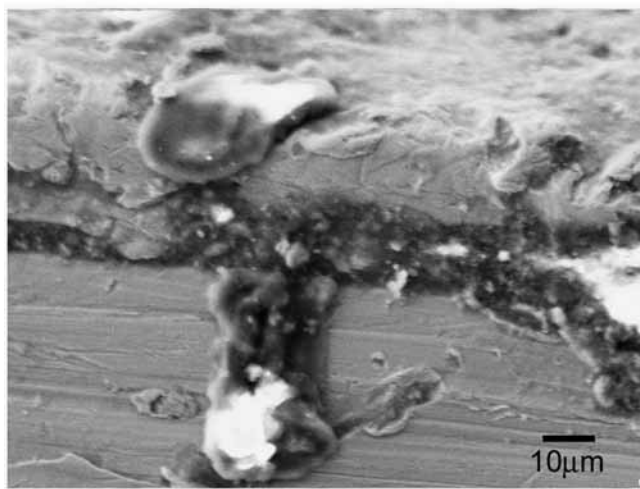
Fig. 9. Hollow stainless steel samples: (a) view at surface, Mag=100×; (b) same region, Mag=300×. Surface appears rough, but no signs of corrosion damage were observed.



(a)

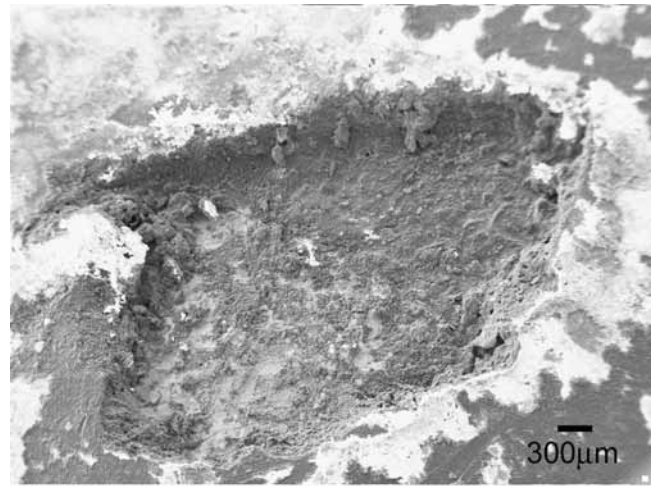


(b)

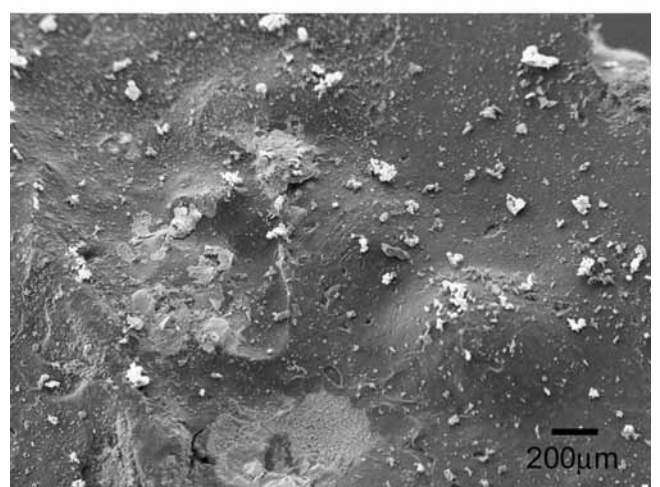


(c)

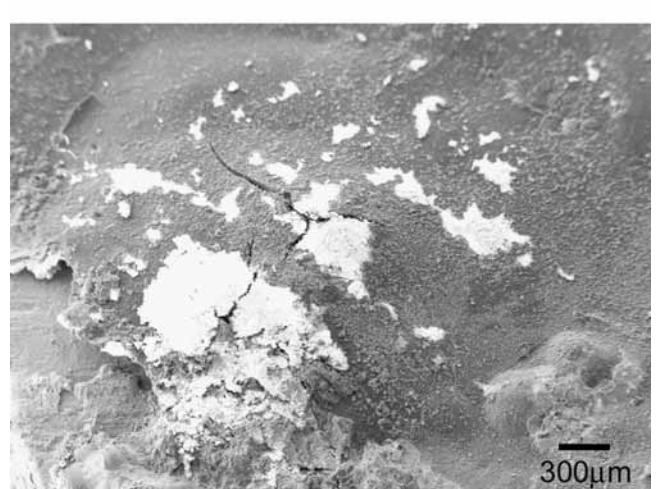
Fig. 10. Stainless steel clad samples: (a) aspect of corrosion along surface, in region close to end of dowel, Mag=100×; (b) details of corrosion at surface, interface between sound and corroded area, Mag=2390×; and (c) detail of corrosion at edge, Mag=2320×



(a)

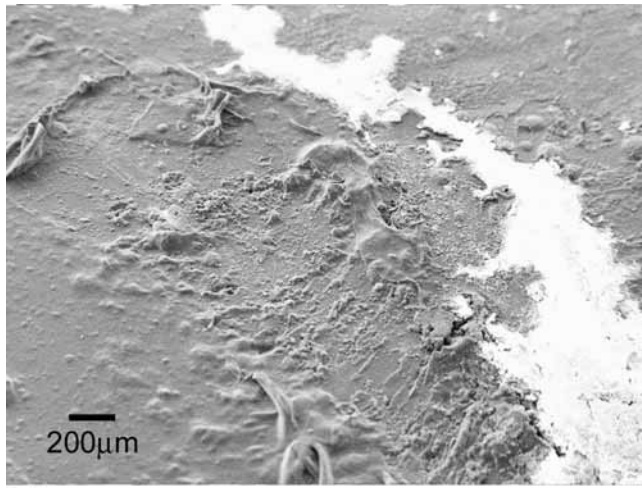


(b)

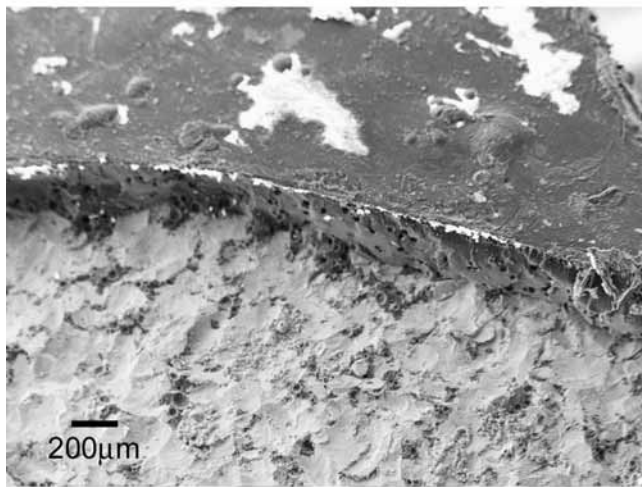


(c)

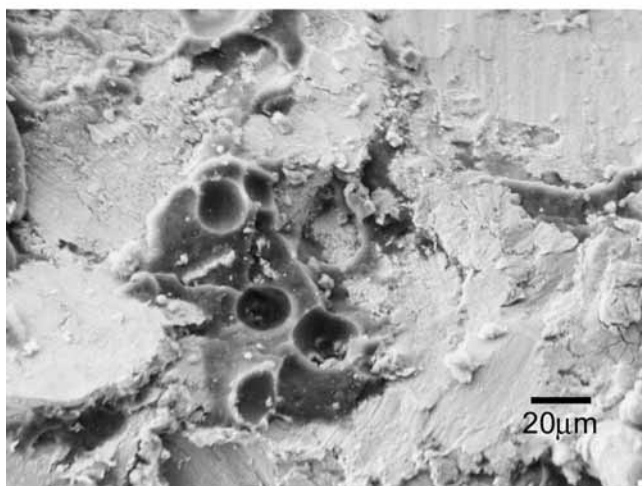
Fig. 11. Gray-epoxy coated samples: (a) view of defect in coating, with corroded area inside, Mag=50×; (b) another region, at edge, where coating is lifted, Mag=75×; and (c) general view of surface, Mag=100×



(a)



(b)



(c)

Fig. 12. Green-epoxy coated samples: (a) general view of surface, Mag=100×; (b) region where part of epoxy coating was stripped off, Mag=100×; and (c) detail of corroded area and pits present under coating, Mag=1330×

highly localized corrosion patterns affect the long-term performance of these dowels warrants further investigation.

Summary and Conclusions

This study investigated the corrosion performance of several types of steel dowels cast in concrete beams using accelerated laboratory tests. Corrosion was accelerated by ponding a concentrated chloride solution on the top of the concrete beams, which had an open “joint” that provided direct access to a short, central segment of the dowels. The following conclusions are based on the results of half-cell potential tests, linear polarization resistance curves, visual inspections, and SEM investigation:

1. The carbon steel dowels exhibited the lowest values of polarization resistance (R_p) and therefore have the smallest resistance to charge transfer across the interface, and consequently present the smallest corrosion resistance;
2. Microcomposite steel dowels exhibited average polarization resistance approximately 35 times larger than carbon steel dowels, while stainless clad and stainless hollow bars had about 73 times greater polarization resistance. This indicates that the microcomposite steel dowels exhibit much greater resistance to corrosion propagation than carbon steel dowels, but not as much as the stainless clad and stainless hollow bars;
3. In epoxy-coated specimens, corrosion is not uniform, but is instead concentrated at localized defective areas (such as pinholes, voids, etc.). Given that epoxy is an electrical insulator, polarization happens only at very small areas (defective regions) that cannot be accounted for in the calculation of the polarization resistance term. Therefore, the epoxy-coated dowels cannot be quantitatively evaluated with the other dowels and must be evaluated qualitatively;
4. Based on corrosion current density results, the carbon steel dowels exhibited very rapid corrosion, while microcomposite steel exhibited a moderate level and stainless steel clad and stainless steel hollow proceeded at a low corrosion rate;
5. Visual inspections of the corroded dowels revealed heavy and mostly uniform corrosion along the carbon steel dowels, light corrosion in the microcomposite steel dowels, and no visible corrosion in the stainless steel clad and stainless steel hollow bars. For the epoxy coated dowels, the visual inspections generally revealed that visible corrosion was not widespread, but did occur at a few localized defective areas, generally at holidays and at the edges of the bar ends. No significant difference was observed on the performance of nonflexible and flexible epoxy-coated dowels; and
6. In general, the microscopic investigation matches the results anticipated by the electrical measurements and visual inspections. The analysis has focused mostly on the corroded regions of each sample, and revealed corroded areas that were not visible to the naked eye.

Acknowledgments

This work was performed with support from the California Department of Transportation (Caltrans), Division of Research and Innovation. Technical assistance was also provided by the Cali-

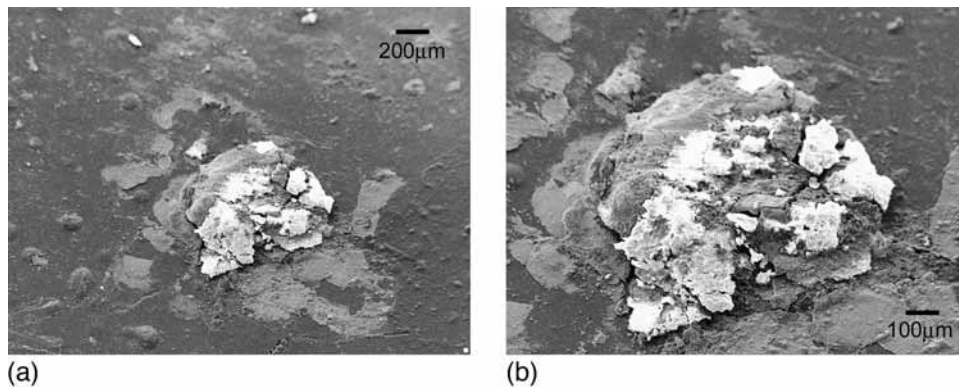


Fig. 13. Purple-epoxy coated samples: (a) general view of surface with corrosion products accumulated in holiday, Mag=100×; (b) zoom in same region, Mag=200×

ifornia DOT Transportation Laboratory. This work represents the opinions of the writers and not necessarily those of the project sponsors.

References

- ASTM. (1999). "Standard test method for half-cell potentials of uncoated reinforcing steel in concrete." *C876*, West Conshohocken, Pa.
- ASTM. (2003). "Standard test method for conducting potentiodynamic polarization resistance measurements." *G59*, West Conshohocken, Pa.
- ASTM. (2004). "Standard specification for epoxy-coated prefabricated steel reinforcing bars." *A934*, West Conshohocken, Pa.
- ASTM. (2007a). "Standard specification for epoxy-coated steel reinforcing bars." *A775*, West Conshohocken, Pa.
- ASTM. (2007b). "Standard test methods for holiday detection in pipeline coatings." *G62*, West Conshohocken, Pa.
- Broomfield, J. P. (1997). *Corrosion of steel in concrete: Understanding, investigation, and repair*, E & FN Spon, London.
- Carino, N. J. (1999). "Nondestructive techniques to investigate corrosion status in concrete structures." *J. Perform. Constr. Facil.*, 13(3), 96–106.
- Harvey, J. T., et al. (2003). "Construction and test results from dowel bar retrofit HVS test sections 553FD, 554FD, and 555FD: US 101, Ukiah, Mendocino County." *Rep. No. UCPRC-RR-2003-03*, Pavement Research Center, Institute of Transportation Studies, Univ. of California, Berkeley, Calif.
- Trejo, D. (1997). "Microstructural design and electrochemical evaluation of microcomposite ferritic martensitic steel for concrete reinforcement." Ph.D. dissertation, Univ. of California, Berkeley, Calif.
- Trejo, D., Monteiro, P. J. M., Gerwick, B. C., and Thomas, G. (2000). "Microstructural design of concrete reinforcing bars for improved corrosion performance." *ACI Mater. J.*, 97(1), 78–83.
- Tuutti, K. (1982). *Corrosion of steel in concrete*, Swedish Cement and Concrete Research Institute, Stockholm, Sweden.